

Influence of off-Sun-Earth line distance on the accuracy of L1 solar wind monitoring

Stephen E. Milan¹, Jennifer Alyson Carter¹, Gemma E. Bower¹, Amy L Fleetham¹, and Brian J. Anderson²

¹University of Leicester

²John Hopkins Univ.

November 23, 2022

Abstract

Upstream solar wind measurements from near the L1 Lagrangian point are commonly used to investigate solar wind-magnetosphere coupling. The off-Sun-Earth line distance of such solar wind monitors can be large, up to 100 RE. We investigate how the correlation between measurements of the interplanetary magnetic field and associated ionospheric responses deteriorates as the off-Sun-Earth line distance increases. Specifically, we use the magnitude and polarity of the dayside region 0 field-aligned currents (R0 FACs) as a measure of IMF BY-associated magnetic tension effects on newly-reconnected field lines, related to the Svalgaard-Mansurov effect. The R0 FACs are derived from Advanced Magnetosphere and Planetary Electrodynamics Response Experiment (AMPERE) measurements by a principal component analysis, for the years 2010 to 2016. We perform cross-correlation analyses between time-series of IMF BY, measured by the Wind spacecraft and propagated to the nose of the bow shock by the OMNI technique, and these R0 FAC measurements. Typically, in the summer hemisphere, cross-correlation coefficients between 0.6 and 0.9 are found. However, there is a reduction of order 0.1 to 0.15 in correlation coefficient between periods when Wind is close to (within 45 RE) and distant from (beyond 70 RE) the Sun-Earth line. We find a time-lag of around 17 minutes between predictions of the arrival of IMF features at the bow shock and their effect in the ionosphere, irrespective of the location of Wind.

1 **Influence of off-Sun-Earth line distance on the accuracy**
2 **of L1 solar wind monitoring**

3 **S. E. Milan^{1,2*}, J. A. Carter¹, G. E. Bower¹, A. L. Fleetham¹, and B. J.**
4 **Anderson³**

5 ¹Department of Physics and Astronomy, University of Leicester, Leicester, UK.

6 ²Birkeland Centre for Space Sciences, University of Bergen, Norway.

7 ³Johns Hopkins University Applied Physics Laboratory, Laurel, Maryland, USA.

8 **Key Points:**

- 9 • We compare OMNI measurements of IMF B_{γ} by Wind with associated variations
10 in the dayside ionosphere
11 • The cross-correlation between these measurements deteriorates as the off-Sun-Earth
12 line distance of Wind increases
13 • A delay of around 17 minutes is found between OMNI predictions of arrival at the
14 bow shock and the ionospheric response

*Department of Physics and Astronomy, University of Leicester, Leicester LE1 7RH, UK

Corresponding author: Steve Milan, steve.milan@le.ac.uk

Abstract

Upstream solar wind measurements from near the L1 Lagrangian point are commonly used to investigate solar wind-magnetosphere coupling. The off-Sun-Earth line distance of such solar wind monitors can be large, up to $100 R_E$. We investigate how the correlation between measurements of the interplanetary magnetic field and associated ionospheric responses deteriorates as the off-Sun-Earth line distance increases. Specifically, we use the magnitude and polarity of the dayside region 0 field-aligned currents (R0 FACs) as a measure of IMF B_Y -associated magnetic tension effects on newly-reconnected field lines, related to the Svalgaard-Mansurov effect. The R0 FACs are derived from Advanced Magnetosphere and Planetary Electrodynamics Response Experiment (AMPERE) measurements by a principal component analysis, for the years 2010 to 2016. We perform cross-correlation analyses between time-series of IMF B_Y , measured by the Wind spacecraft and propagated to the nose of the bow shock by the OMNI technique, and these R0 FAC measurements. Typically, in the summer hemisphere, cross-correlation coefficients between 0.6 and 0.9 are found. However, there is a reduction of order 0.1 to 0.15 in correlation coefficient between periods when Wind is close to (within $45 R_E$) and distant from (beyond $70 R_E$) the Sun-Earth line. We find a time-lag of around 17 minutes between predictions of the arrival of IMF features at the bow shock and their effect in the ionosphere, irrespective of the location of Wind.

Plain Language Summary

Space weather within the Earth's geospace environment is driven by the interaction of the solar wind with the magnetosphere. Measurements of the solar wind upstream of the Earth are crucial for understanding this interaction and for providing some advanced warning of hazardous conditions about to arrive. Such measurements are typically made by spacecraft located in orbit about the L1 Lagrangian point, sometimes far from the Sun-Earth line, and it is uncertain how representative these measurements are of the solar wind that actually hits the Earth. In this study we investigate how predictions degrade as the off-Sun-Earth line distance increases. We use measurements of the east-west component of the interplanetary magnetic field measured by the Wind spacecraft and observations of magnetic field-aligned electrical currents within the magnetosphere, to assess how well these are correlated. We find that the correlation does indeed decrease somewhat as Wind wanders far from the Sun-Earth line. This study will help provide confidence in using these upstream monitors, but also allow quantification of what discrepancies can be expected. It also allows the scale-size of features in the solar wind to be estimated.

1 Introduction

Upstream solar wind monitoring is invaluable for studies of the relationship between conditions within the interplanetary medium and dynamics within the Earth's magnetosphere, and for forecasting upcoming geomagnetic activity. Ideally, spacecraft just ahead of the bowshock, or even within the magnetosheath, can give measurements of the plasma characteristics and magnetic field that are about to impinge on the magnetopause. However, orbital dynamics prevent spacecraft station-keeping in such ideal locations, and spacecraft so close to the magnetopause do not provide much advanced warning of incoming space weather hazards. A compromise is to place spacecraft in orbit about the L1 Lagrangian point, such that they can be kept in front of the magnetosphere, providing measurements of the solar wind which will impact the magnetosphere in approximately one hour's time. Such spacecraft have included Wind, the Advanced Composition Explorer (ACE), and the Deep Space Climate Observatory (DSCOVR). Goddard Space Flight Centre developed the OMNI dataset, which assesses the speed and orientation of features within the solar wind measured by these and other spacecraft, and time-lags the obser-

65 vations to the point of impact on the bow shock (King & Papitashvili, 2005). This dataset
 66 has been instrumental in advancing our understanding of the interaction of the solar wind
 67 with the magnetosphere. However, the spacecraft providing these observations can wan-
 68 der up to $100 R_E$ from the Sun-Earth line, such that it is unclear how representative their
 69 measurements are of the solar wind which will actually arrive at the magnetosphere (e.g.,
 70 Crooker et al., 1982; Collier et al., 1998; Case & Wild, 2012). It is the purpose of this
 71 paper to investigate how the predictive capability of solar wind monitoring deteriorates
 72 as the off-Sun-Earth line distance increases.

73 To assess the accuracy of the upstream measurements, some ground-truth is nec-
 74 essary: an observable that is thought to accurately reflect conditions within the solar wind
 75 that is interacting with the magnetopause. In this study we use the Svalgaard-Mansurov
 76 effect, in which field-aligned and ionospheric currents within the cusp region react to the
 77 B_Y component of the interplanetary magnetic field (IMF), and produce DPY magnetic
 78 perturbations on the ground (Svalgaard, 1973; Mansurov, 1969; Friis-Christensen et al.,
 79 1972; Jørgensen et al., 1972; Cowley et al., 1991). Milan et al. (2015, 2017) showed that
 80 principal component analysis (PCA) could be used to automatically extract the polar-
 81 ity and magnitude of the field-aligned currents (FACs) associated with this effect from
 82 observations of the global FAC pattern by the Advanced Magnetosphere and Planetary
 83 Electrodynamics Response Experiment or AMPERE (Anderson et al., 2000, 2002; Wa-
 84 ters et al., 2001, 2020). We refer to this as the region 0 (R0) FAC to distinguish it from
 85 the region 1 and region 2 (R1/R2) FACs first identified by Iijima and Potemra (1976).
 86 Milan et al. (2018) refined the procedure by applying PCA separately to just the day-
 87 side portion of the FAC patterns. They demonstrated that the polarity of the currents
 88 switched promptly when there were sharp reversals in IMF B_Y at the nose of the bow
 89 shock as predicted by OMNI, with a time-lag of between 10 and 20 minutes. This time-
 90 lag is interpreted as the propagation delay associated with traversal of the magnetosheath
 91 by the shocked solar wind and one or two Alfvén travel-times from the magnetopause
 92 to the ionosphere. Moreover, the association between R0 FAC polarity and IMF B_Y held
 93 irrespective of whether IMF B_Z was directed southwards or northwards. Hence, we con-
 94 sider the magnitude and polarity of the R0 FAC, extracted using the PCA technique of
 95 Milan et al. (2018), to be a good indicator of the sense of IMF B_Y at the magnetopause.

96 We perform a cross-correlation analysis between IMF B_Y observed by the Wind
 97 spacecraft and the R0 FAC extracted from AMPERE data for the period 2010 to 2016.
 98 The Wind spacecraft orbited the L1 point in an elliptical orbit varying periodically in
 99 off-Sun-Earth line distance, $R_{YZ} = (Y^2 + Z^2)^{1/2}$, between $30 R_E$ and $100 R_E$, where
 100 Y and Z are GSE coordinates. We determine how the cross-correlation deteriorates as
 101 R_{YZ} increases.

102 2 Methodology and observations

103 AMPERE inverts magnetic perturbations observed by the 66 spacecraft of the Irid-
 104 ium constellation to determine the global distribution of field-aligned currents (FACs)
 105 across the northern and southern hemispheres on a geomagnetic grid with 24 magnetic
 106 local time (MLT) sectors and 50 one-degree magnetic colatitude bins, with a cadence of
 107 2 minutes (Anderson et al., 2000, 2002; Waters et al., 2001; Coxon et al., 2018). The mor-
 108 phology of the FACs responds to changes in upstream solar wind and IMF conditions,
 109 to changes in magnetotail processes, and to changes in the magnetic open flux content
 110 of the magnetosphere (Clausen et al., 2012; Milan et al., 2018). Analysing this feature-
 111 rich dataset can be difficult. As an exercise in dimensionality-reduction, Milan et al. (2015)
 112 applied principal component analysis (PCA) to the FAC patterns to find the set of basis-
 113 vectors (“eigenFACs”) that best represent the variability within the data. It was found
 114 that the most significant eigenFAC represented the R1/R2 current system (Iijima & Potemra,
 115 1976) and the second-most the R0 system. The analysis was improved by Milan et al.
 116 (2018) in that FACs sunwards and antisunwards of the dawn-dusk meridian were anal-

117 ysed separately, and two sets of eigenFACs computed, recognising that dayside and night-
 118 side processes are largely decoupled. It is this second method that we employ in this study,
 119 concentrating solely on the dayside FACs.

120 The PCA technique is described in detail by Milan et al. (2015, 2018), but we reprise
 121 it here briefly for completeness. Each 2-min AMPERE map comprises 1200 FAC den-
 122 sity values on a 25×50 grid. First, each map is normalised to remove the influence of
 123 changing polar cap size (Clausen et al., 2012): the centre of the FAC pattern is found,
 124 a circle is fitted to the boundary between the R1 and R2 FACs, and then each map is
 125 rescaled to a common size. Each pre-processed map (of which there are nearly two mil-
 126 lion for each hemisphere) is represented as a vector of data values and all the individ-
 127 ual vectors are stacked together to form a matrix. This matrix is multiplied by its trans-
 128 pose to find the covariance matrix of the dataset. The eigenvectors of this covariance ma-
 129 trix are the dominant patterns of variability within the data (the eigenFACs) and their
 130 corresponding eigenvalues indicate their significance in explaining this variability. To find
 131 the contribution of a particular eigenFAC to an individual map, the inner product or “over-
 132 lap” between the two is computed: in the case of the second eigenFAC, which corresponds
 133 to the R0 FAC system, this overlap is referred to as α_2 (which has arbitrary units). This
 134 then formed our primary magnetospheric observable. Measurements from both the north-
 135 ern and southern hemispheres (NH and SH) were available.

136 The OMNI dataset employs observations from a range of upstream solar wind mon-
 137 itors to predict the solar wind and IMF conditions at the nose of the bow shock by com-
 138 puting an expected propagation delay from the spacecraft location and time-lagging the
 139 data. A long time-series of standard OMNI data may come from several different space-
 140 craft located at different distances from the magnetosphere. However, the OMNI data-
 141 portal also provides access to data from an individual spacecraft ([https://omniweb.gsfc](https://omniweb.gsfc.nasa.gov/ow_min.html)
 142 [.nasa.gov/ow_min.html](https://omniweb.gsfc.nasa.gov/ow_min.html)): to simplify analysis, in this study we use data from Wind alone.
 143 The primary parameter we used is the GSM B_Y component of the IMF. This is provided
 144 at 1-min cadence, but we down-sampled this to 2-min to match the AMPERE observa-
 145 tions.

146 Figure 1 shows the dependence of NH α_2 on IMF B_Y for the period 2010 to 2016,
 147 subdivided by month. A clear positive linear correlation between the two is found, in-
 148 dicated that the polarity and magnitude of the R0 FACs is controlled by B_Y -related ten-
 149 sion forces on newly-reconnected field lines. This is clearly true for both northwards and
 150 southwards IMF conditions. The slope of the fit is greatest in summer months and be-
 151 comes almost zero in January and December. This seasonal dependence is thought to
 152 be mainly controlled by the ionospheric conductance at the footprint of the R0 FACs,
 153 produced by solar illumination. As the conductance increases in summer there is greater
 154 frictional coupling between the ionosphere and neutral atmosphere, and hence more in-
 155 tense FACs are required to transmit stress from the magnetopause to the ionosphere. How-
 156 ever, as noted by Milan et al. (2001), East-West variations in the dayside ionospheric con-
 157 vection throat are less pronounced in winter than in summer, so the R0 seasonal vari-
 158 ation may also reflect hemispheric differences in dayside solar wind-magnetosphere-ionosphere
 159 coupling. We use α_2 , especially in summer months as an indicator of IMF B_Y at the mag-
 160 netopause. Similar results are found for the SH (not shown), except that the slope is neg-
 161 ative as the polarity of the SH R0 FACs is opposite to the sense of B_Y . In this case, the
 162 slope of the relationship maximises in SH summer, i.e., December and January, though
 163 the slope is weaker in the SH than in the NH. It is known that the SH FACs are in gen-
 164 eral weaker than in the NH (Coxon et al., 2016; Milan et al., 2017), and this is borne out
 165 in these results.

166 Any small gaps in the α_2 and B_Y time-series were linearly interpolated over. We
 167 divided the α_2 and B_Y time-series into separate windows, each N data-points in length,
 168 and calculated the cross-correlation between the two, noting the peak correlation coef-
 169 ficient value and the lag at which this peak occurred. The analysis was then repeated,

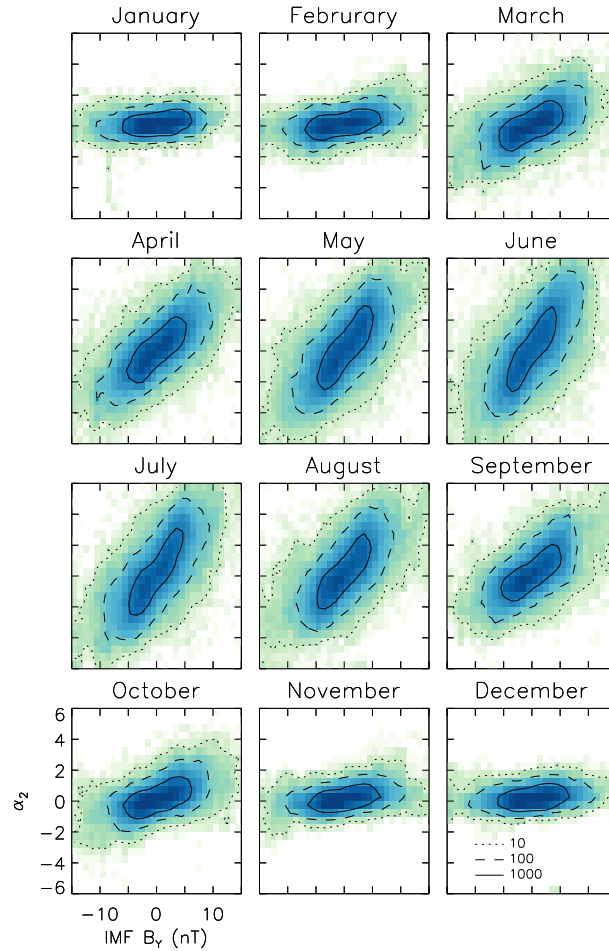


Figure 1. The occurrence distributions showing the relationship between the northern hemisphere α_2 coefficient and IMF B_Y in bins 1 nT wide and 0.5 (arbitrary units) high, for the months January to December, 2010 to 2016. The occurrence is shown on a logarithmic scale, contours indicating 10, 100, and 1000 occurrences per bin.

170 with the window stepped on by $N/2$ data-points each time, for the 7-year period (2010
 171 to 2016) for which AMPERE data is currently available. We selected the optimum value
 172 of N by trying a range of different values. Values of N between approximately 500 and
 173 900 maximised the cross-correlation, with a broad peak. We selected $N = 720$ (1 day)
 174 because this meant that dipole angle (controlling solar insolation of the cusp region iono-
 175 sphere) averaged out over the window. Smaller values of N would have lead to diurnal
 176 variations in the cross-correlation coefficient. With $N = 720$, there were 5114 possible
 177 cross-correlation windows; once data gaps from Wind or AMPERE were factored in, 4587
 178 remained. We note that the exact choice of N does not alter the subsequent findings of
 179 this study.

180 The results of the analysis for the NH are presented in Figure 2. The top panel shows
 181 the maximum correlation coefficient from the cross-correlation analysis in grey; a 10-day
 182 (20-point) running mean is shown in black. The middle panel shows the lag with the max-
 183 imum correlation, with the marginal distribution shown to the right. The bottom panel
 184 shows the location of the Wind spacecraft in GSE coordinates. The spacecraft was in
 185 an elliptical orbit about L1, varying in X between approximately 200 and 260 R_E , in
 186 Z between $\pm 20 R_E$, and in Y between $\pm 100 R_E$. As a consequence, the distance off the
 187 Sun-Earth line, $R_{YZ} = (Y^2 + Z^2)^{1/2}$, varied between approximately 25 and 100 R_E ,
 188 about 4 times a year.

189 The peak correlation between α_2 and B_Y varied between 0.9 and -0.2 (the running
 190 mean between 0.8 and 0.2), maximising in summer months due to the R0 current mag-
 191 nitudes being greatest at these times. The running mean was close to 0.7 in summer. The
 192 lag of peak correlation showed a broad peak between 10 and 30 mins, with a maximum
 193 near 17 mins; the range increased in winter months when the correlation coefficient was
 194 small and clustered near 17 mins in summer months (with a few exceptions, see below).
 195 In the top panel, vertical, red dashed lines show the times when R_{YZ} maximised, and
 196 there appears to be, on average, a reduction in the running-mean of the correlation co-
 197 efficient by about 0.1 at these times.

198 A Fourier analysis of the correlation time-series indicates peaks in the spectrum
 199 at 365 days (1 year), 183 days (half a year), 150 days, and 88 days (the frequency of vari-
 200 ation of R_{YZ}). A reconstruction of the time-series using the first 3 peaks is shown in green
 201 (offset for clarity) and including the 88 day component in blue. Although the effect is
 202 small, there is clearly a reduction in the correlation around the maxima in R_{YZ} . The
 203 365 day period reflects the seasonal variation in the correlation and the 183 day period
 204 appears as the summer maxima are wider than the winter minima. It is unclear what
 205 gives rise to the 150 day period.

206 Ten representative intervals, along with their peak correlation and peak lag, have
 207 been highlighted by red dots. The associated IMF B_Y (red) and α_2 (black) time-series
 208 are presented in Figure 3. In the majority of cases there is a close correspondence be-
 209 tween B_Y and the polarity and magnitude of the R0 FAC. However, each panel high-
 210 lights some typical features within the correlations which we now discuss.

211 (a) The correlation is high, but at times the variation in the R0 FAC appears to
 212 precede those in B_Y , and a peak lag of -12 mins is found. (b) Variations in B_Y are rapid
 213 and some short-duration features are not well-captured by α_2 ; this may indicate a smooth-
 214 ing effect in the magnetospheric response to rapid B_Y changes. A time-lag of 18 mins
 215 is found. (c) In this example, short-duration negative excursions in B_Y are also present
 216 in α_2 , with a consistent time-lag near 16 mins. (d) Although there are significant vari-
 217 ations in B_Y , α_2 is near-zero throughout; this interval comes from near the winter sol-
 218 stice, when the R0 FAC is almost absent from the dayside currents. (e) There are rel-
 219 atively long duration changes in B_Y ; although some of these excursions are present also
 220 in α_2 , some features are absent, for example around data points 200 and 360, and as a
 221 consequence a relatively long time lag of 24 mins is found. (f) Overall, the correlation

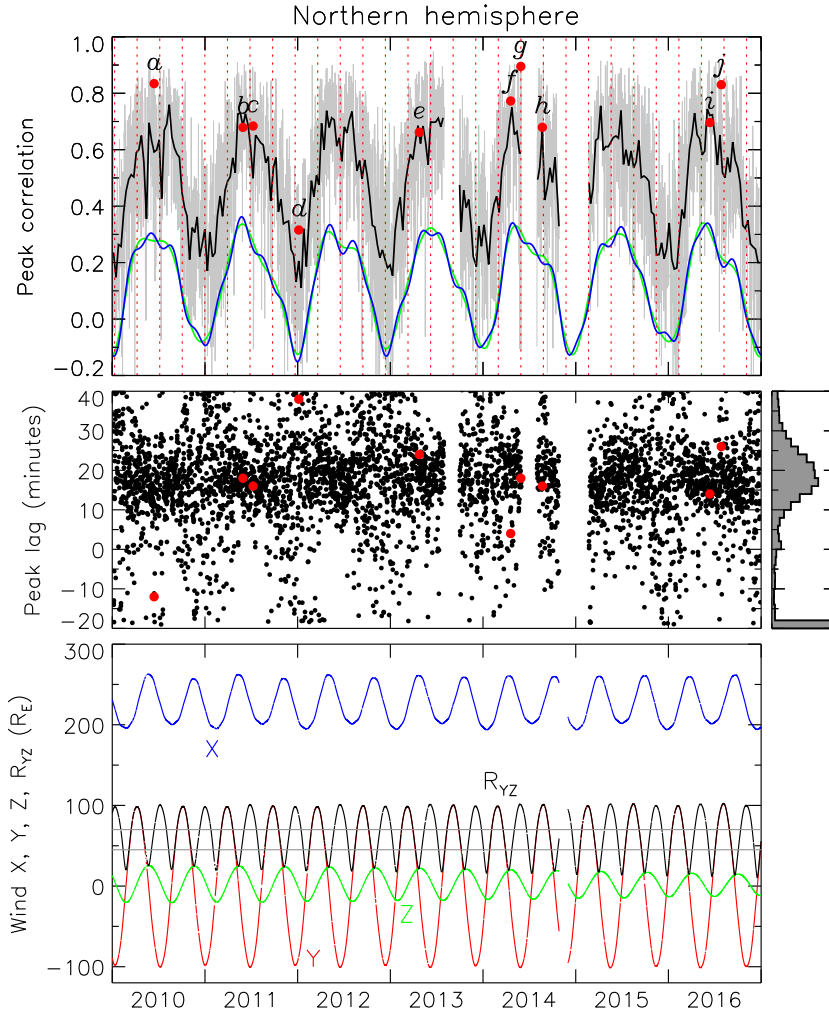


Figure 2. (Top) The peak cross-correlation coefficient between NH α_2 and IMF B_Y every 12 hours (grey), and a 10-day running mean (black). The green and blue curves are reconstructions of the correlation time series using a Fourier expansion in 3 and 4 terms, respectively (see text for details), displaced vertically for clarity. Vertical red, dashed lines indicate times that the Wind spacecraft was furthest from the Sun-Earth line. (Middle) The lag associated with the peak in the cross-correlation. The marginal distribution is shown to the right; the bottom bar indicates the proportion of correlations in which the lag of peak correlation was outside the -20 to 40 min range. (Bottom) The position of the Wind spacecraft in GSE X (blue), Y (red), and Z (green). The distance from the Sun-Earth line, R_{YZ} is shown in black. Red dots in the figure correspond to panels in Figure 3.

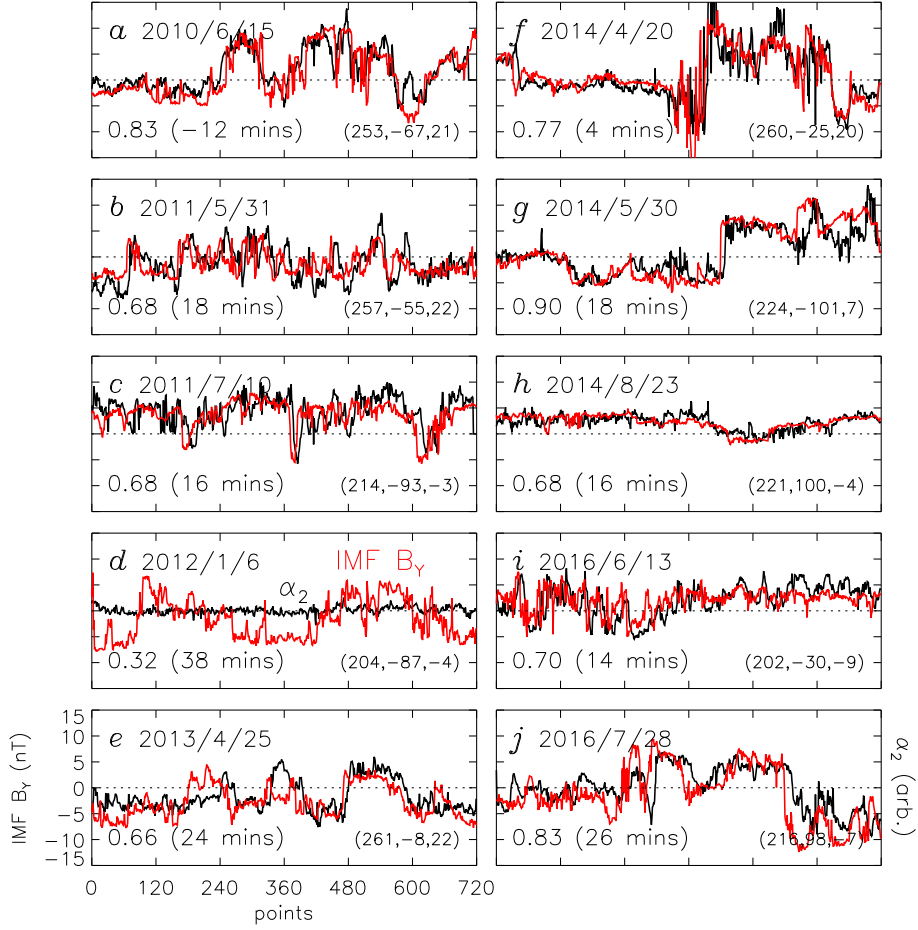


Figure 3. Ten selected correlations, highlighted by red dots in Figure 2. Each panel corresponds to 24 hours of data (720 data points). IMF B_Y (GSM) observed at Wind is shown in red, the α_2 parameter in black; α_2 is shown on an arbitrary scale, though it is the same in each panel. The top-left in each panel indicates the date of the observations, the bottom-left the peak correlation coefficient and peak lag, and the bottom-right the approximate (X, Y, Z) GSE coordinates of Wind.

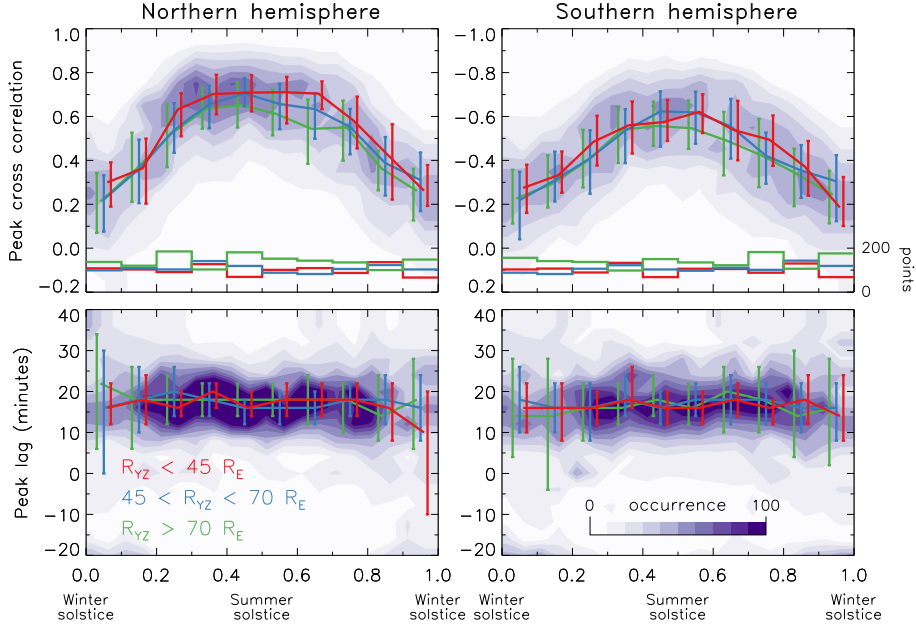


Figure 4. Combined seasonal dependence of peak cross-correlation (top panels) and peak lag (bottom panels) between IMF B_Y and α_2 , for the years 2010 to 2016 in the northern hemisphere (left panels) and southern hemisphere (right panels). Shading shows the overall occurrence distribution. The median and quartiles of the distributions for off-Sun-Earth line distances $R_{YZ} < 45R_E$, $45 < R_{YZ} < 70R_E$, and $R_{YZ} > 70R_E$ are shown in red, blue, and green. The number of points in each year-fraction bin is indicated in the lower portion of the top panels.

222 is high but although there is a clear lag between B_Y and α_2 at the start of the interval,
 223 no lag is apparent at the end, and an overall lag of 4 mins is found. (g) The overall cor-
 224 relation is high, but some discrepancy is seen after data point 540. (h) Only slow vari-
 225 ations in B_Y are seen at Wind and these are reflected in α_2 . (i) Some rapid fluctua-
 226 tions in B_Y are not present in α_2 and towards the end of the interval some fluctua-
 227 tions are seen in α_2 but not B_Y . (j) Long-duration variations in B_Y are also seen in α_2 , but the
 228 timings are quite variable, and a relatively long lag is calculated.

229 Figure 4 shows the correlation data, peak correlation in the top panels and peak
 230 lag in the bottom panels, for both the northern and southern hemispheres as a function
 231 of time of year (year-fraction from winter solstice to winter solstice). The shading shows
 232 the occurrence distribution of the full data set. The data are then subdivided by the dis-
 233 tance of Wind from the Sun-Earth line, R_{YZ} , in ranges of less than $45 R_E$ (red), be-
 234 tween 45 and $70 R_E$ (blue), and greater than $75 R_E$ (green). These ranges were selected such
 235 that similar numbers of correlations fell in 10 equal-width year-fraction bins (the occur-
 236 rences are shown in the lower portions of the top panels); these ranges are shown as hori-
 237 zontal grey lines in the lower panel of Figure 2. The median and upper and lower quar-
 238 tiles of peak correlation and peak lag are then calculated in each bin, and shown as the
 239 coloured curves and vertical bars. The peak correlations in the NH and SH are positive
 240 and negative, respectively, due to the polarity of the R0 FACs in the two hemispheres.

241 The correlations are a minimum in winter and a maximum in summer, due to the
 242 weakness of the R0 FACs when there is little solar insolation. The median peak cor-
 243 relation in summer is 0.7 in the NH and 0.6 in the SH; the summer NH peak is higher and
 244 broader than that in the SH. We attribute the discrepancy between the two hemispheres
 245 to two factors: (a) it is known that the FACs measured by AMPERE are overall weaker

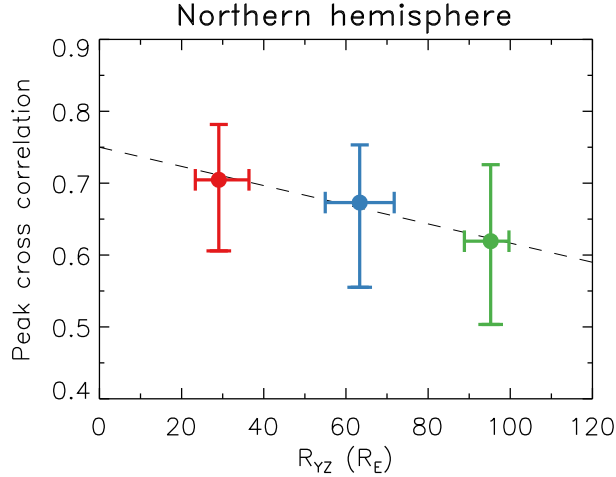


Figure 5. The reduction in median peak correlation with off-Sun-Earth line distance, R_{YZ} . Vertical and horizontal bars show the quartiles within the bins $R_{YZ} < 45R_E$, $45 < R_{YZ} < 70R_E$, and $R_{YZ} > 70R_E$. Only correlations between year-fractions of 0.3 and 0.7 are included in the analysis.

246 in the SH than the NH (Coxon et al., 2016; Milan et al., 2017), though the reasons for
 247 this are still unknown; (b) the orbital configuration of the Iridium spacecraft is sub-optimal
 248 in the SH (Waters et al., 2020), such that small-scale FACs (including R0) may be poorly
 249 sampled. The peak lag distribution maximises near 17-18 minutes at all times of year,
 250 though it broadens around winter solstice when the correlations are poor.

251 Our main finding is that the peak correlation depends on R_{YZ} , such that as Wind
 252 moves further from the Sun-Earth line the correlation decreases, especially in the NH.
 253 We focus on year-fractions between 0.3 and 0.7, the broad summer maximum. The dif-
 254 ference in the median correlation coefficient between the $R_{YZ} < 45R_E$ and $R_{YZ} > 70R_E$
 255 bins is of order 0.1, as seen in Figure 5. The difference between the upper and lower quar-
 256 tiles also increases marginally with greater R_{YZ} . A linear fit to the data suggests that
 257 if measurements were available at $R_{YZ} = 0$, then the decrease in correlation coefficient
 258 at $R_{YZ} = 100R_E$ would be of order 0.15. On the other hand, there is little discernible
 259 difference in the peak lags in the different R_{YZ} ranges.

260 Similar analyses were attempted, expect binning the data by Wind X or Y . Un-
 261 fortunately, the period of the Wind orbit, being close to 6 months, precluded a uniform
 262 sampling across the different seasons. What results were obtained suggested that the up-
 263 stream distance, X , makes little difference to the correlations, and that the Y location,
 264 either ahead of Earth in its orbit or behind, did not change the results found in Figure
 265 4.

266 3 Discussion and Conclusions

267 There has been debate regarding the validity of L1 observations of the solar wind
 268 for understanding solar wind-magnetosphere coupling, especially when monitors are a
 269 long distance from the Sun-Earth line. We have used the magnitude and polarity of the
 270 R0 field-aligned currents derived from AMPERE observations as ground-truth for the
 271 predictions by OMNI (specifically from the Wind spacecraft) of the B_Y component of
 272 the IMF that impacts the magnetosphere. The measured parameter we have used is the
 273 α_2 component derived from a principal component analysis of the FACs (Milan et al.,

274 2015, 2017, 2018). This ground-truth is only applicable in summer months as the R0 FACs
 275 are weak around winter solstice due to a lack of solar insolation and a possible seasonal
 276 dependence in the East-West asymmetry of the dayside convection throat (Milan et al.,
 277 2001). We have shown that the cross-correlation between IMF B_Y and α_2 decreases as
 278 the off-Sun-Earth line distance, R_{YZ} , increases. The reduction in peak cross-correlation
 279 coefficient is around 0.1 to 0.15. We also find a relatively consistent time-lag between
 280 variations in IMF B_Y and α_2 of between 15 and 20 minutes on average. This lag is in-
 281 terpreted as the communication-time between solar wind changes at the bow shock (the
 282 predicted timing given by the OMNI technique) and the ionosphere, comprising the prop-
 283 agation delay across the magnetosheath and some Alfvén travel-time from the magne-
 284 topause and the ionosphere. Significantly longer or shorter time lags, or even negative
 285 time lags (Figure 3a), indicate that an incorrect propagation delay was calculated by the
 286 OMNI technique. Such discrepancies could be produced by the assumption that solar
 287 wind features have planar boundaries, especially if R_{YZ} is large. However, we do not see
 288 a significant change in timing with R_{YZ} .

289 Khan and Cowley (1999) estimated that the delay between solar wind features arriv-
 290 ing at the bow shock nose and the associated response in the ionosphere should be
 291 of order 5 to 15 mins, possibly with some systematic offset. Our finding of a delay of 15
 292 to 20 mins could indicate that this systematic offset is approximately 10 mins. It may
 293 also reflect the time that the R0 FACs take to respond to changes in IMF B_Y , occupy-
 294 ing as they do an area in the ionosphere of up to 10° of latitude by 3-4 hours of MLT
 295 (Milan et al., 2015). Alternatively, the systematic delay could be due to the AMPERE
 296 technique itself, in which the Iridium spacecraft take approximately 10 mins to traverse
 297 their $\sim 30^\circ$ latitudinal separation around each orbital plane.

298 While many studies have focussed on the timing of solar wind features (Crooker
 299 et al., 1982; Collier et al., 1998; Case & Wild, 2012), here we have mainly studied the
 300 fidelity between solar wind measurements from far upstream and the response within the
 301 magnetosphere; in other words, these correlations have been filtered through the solar
 302 wind-magnetosphere coupling process. Despite this, the correlations can be high (of or-
 303 der 0.9) even when rapid and short duration fluctuations appear in IMF B_Y , indicat-
 304 ing that the magnetospheric response can be prompt and linear, during both northwards
 305 and southwards IMF conditions. In general, the median correlation is about 0.7 in sum-
 306 mer months, indicating that the response is not always so exact. The results reported
 307 are clearer in the northern hemisphere than in the southern hemisphere, though we an-
 308 ticipate that this is due to stronger FACs being observed in the NH and a less optimal
 309 orbital configuration of AMPERE in the SH. This does suggest, however, that the cor-
 310 relation coefficients will be limited by the spatial and temporal resolution of the AM-
 311 PERE technique and our method of extracting the R0 FACs from a complicated data
 312 set.

313 Putting limitations of the technique to one side, lower correlation coefficients can
 314 arise for several reasons, including a lack of fidelity between measurements at L1 and in
 315 the ionosphere, i.e. short-duration features that are seen in B_Y but not in α_2 and *vice*
 316 *versa* (e.g., Figure 3e and i), or changes in the lag between the two within a 24 hour win-
 317 dow (e.g., Figure 3a and f). However, individual cases of these discrepancies are not nec-
 318 essarily due to large R_{YZ} : high correlations can be found when Wind is far from the Sun-
 319 Earth line (Figure 3a and g) and poorer correlations when Wind is near the Sun-Earth
 320 line (Figure 3e). Visual inspection of Figure 2 does seem to suggest that there are dips
 321 in correlation correlation of about 0.1 to 0.2 when Wind is at it's maximum distance from
 322 the Sun-Earth line, though the temporal width of these dips is quite variable. This cor-
 323 roborates the changes in median correlation with increasing R_{YZ} shown in Figures 4 and
 324 5.

325 Collier et al. (1998) studied the solar wind propagation delay from a spacecraft far
 326 upstream of the Earth and one just outside the bow shock. By comparing their timings

with similar ones made by Crooker et al. (1982), they suggested that there might be a solar cycle dependence of the orientation of features in the solar wind and hence the accuracy of predicted propagation delay. However, although our observations span over half a solar cycle (albeit a relatively weak cycle), from examination of Figure 2 we see no evidence for such a dependence in our correlations.

R_{YZ} varies between about 25 and 100 R_E . The reduction in correlation when R_{YZ} is large suggests that there is structure within the solar wind transverse to the flow direction on spatial scales of 100 R_E . Crooker et al. (1982) estimated the coherence scale length of features in the solar wind to be of order 90 R_E , which is approximately consistent with our findings. On the other hand, the structure along the flow direction is known to be as small as 10 R_E , corresponding to temporal variations in the OMNI data of a few minutes.

Many authors have developed coupling functions for the solar wind-magnetosphere interaction (e.g., Newell et al., 2007; Milan et al., 2012; Lockwood & McWilliams, 2021, and references therein). Accurate characterisation of the upstream solar wind conditions is crucial for such studies. The problems with solar wind monitors identified in the present study suggests that there is an intrinsic limit to the predictive capability of such coupling functions.

A similar study could have been undertaken with ground-based magnetometers, looking for magnetic perturbations produced by the horizontal ionospheric closure currents associated with the R0 FACs, or ionospheric radars looking at the east-west sense of the dayside convection throat. Both methods would have suffered from non-continuous data (neither magnetometers nor radars remain located in the cusp sector), and it would have been much less straightforward to remove the effect of latitudinal changes in the position of the cusp. We have also been able to exploit the fact that the polarity of the R0 FACs seems independent of whether the IMF is directed northwards or southwards, whereas the convection geometry changes markedly under these two conditions.

We conclude that solar wind measurements up to 100 R_E off the Sun-Earth line are valuable for studies of solar wind-magnetosphere coupling. Discrepancies between IMF variations and their ground signature, and the timing between these, can be found for all values of R_{YZ} . However, a reduction in the overall fidelity of predictions of IMF features does occur as this distance increases. We have quantified this as a reduction in cross-correlation coefficient between measurements near L1 and in the ionosphere of between 0.1 and 0.15 in time-series of 24 hour duration.

Acknowledgments

SEM and JAC were supported by the Science and Technology Facilities Council (STFC), UK, grant no. ST/S000429/1; GEB and ALF were supported by STFC studentships. The work at the Birkeland Centre for Space Centre, University of Bergen, Norway, was supported by the Research Council of Norway/CoE under contract 223252/F50. We thank the AMPERE team and the AMPERE Science Center for providing the Iridium-derived data products; AMPERE products are available at <http://ampere.jhuapl.edu>. The OMNI data were obtained from the GSFC/SPDF OMNIWeb interface at <http://omniweb.gsfc.nasa.gov>.

References

- Anderson, B., Takahashi, K., Kamei, T., Waters, C., & Toth, B. (2002). Birkeland current system key parameters derived from Iridium observations: Method and initial validation results. *Journal of Geophysical Research: Space Physics*, 107(A6), SMP-11. doi: <https://doi.org/10.1029/2001JA000080>
- Anderson, B., Takahashi, K., & Toth, B. (2000). Sensing global Birkeland currents

- 376 with Iridium® engineering magnetometer data. *Geophysical Research Letters*,
 377 27(24), 4045–4048. doi: <https://doi.org/10.1029/2000GL000094>
- 378 Case, N., & Wild, J. (2012). A statistical comparison of solar wind propagation de-
 379 lays derived from multispacecraft techniques. *Journal of Geophysical Research:*
 380 *Space Physics*, 117(A2). doi: <https://doi.org/10.1029/2011JA016946>
- 381 Clausen, L., Baker, J., Ruohoniemi, J., Milan, S., & Anderson, B. (2012). Dy-
 382 namics of the region 1 Birkeland current oval derived from the Active Mag-
 383 netosphere and Planetary Electrodynamics Response Experiment (AM-
 384 PERE). *Journal of Geophysical Research: Space Physics*, 117(A6). doi:
 385 <https://doi.org/10.1029/2012JA017666>
- 386 Collier, M. R., Slavin, J., Lepping, R., Szabo, A., & Ogilvie, K. (1998). Tim-
 387 ing accuracy for the simple planar propagation of magnetic field structures
 388 in the solar wind. *Geophysical Research Letters*, 25(14), 2509–2512. doi:
 389 <https://doi.org/10.1029/98GL00735>
- 390 Cowley, S., Morelli, J., & Lockwood, M. (1991). Dependence of convective
 391 flows and particle precipitation in the high-latitude dayside ionosphere
 392 on the x and y components of the interplanetary magnetic field. *Jour-*
 393 *nal of Geophysical Research: Space Physics*, 96(A4), 5557–5564. doi:
 394 <https://doi.org/10.1029/90JA02063>
- 395 Coxon, J., Milan, S., & Anderson, B. (2018). A review of Birkeland current research
 396 using AMPERE. *Electric Currents in Geospace and Beyond*, 257–278. doi:
 397 <https://doi.org/10.1002/9781119324522.ch16>
- 398 Coxon, J., Milan, S., Carter, J., Clausen, L., Anderson, B., & Korth, H. (2016).
 399 Seasonal and diurnal variations in AMPERE observations of the Birkeland
 400 currents compared to modeled results. *Journal of Geophysical Research: Space*
 401 *Physics*, 121(5), 4027–4040. doi: <https://doi.org/10.1002/2015JA022050>
- 402 Crooker, N., Siscoe, G., Russell, C., & Smith, E. (1982). Factors controlling degree
 403 of correlation between isee 1 and isee 3 interplanetary magnetic field measure-
 404 ments. *Journal of Geophysical Research: Space Physics*, 87(A4), 2224–2230.
 405 doi: <https://doi.org/10.1029/JA087iA04p02224>
- 406 Friis-Christensen, E., Lassen, K., Wilhjelm, J., Wilcox, J., Gonzalez, W., & Colburn,
 407 D. (1972). Critical component of the interplanetary magnetic field responsible
 408 for large geomagnetic effects in the polar cap. *Journal of Geophysical Research*,
 409 77(19), 3371–3376. doi: <https://doi.org/10.1029/JA077i019p03371>
- 410 Iijima, T., & Potemra, T. (1976). The amplitude distribution of field-aligned cur-
 411 rents at northern high latitudes observed by Triad. *Journal of Geophysical Re-*
 412 *search*, 81(13), 2165–2174. doi: <https://doi.org/10.1029/JA081i013p02165>
- 413 Jørgensen, T. S., Friis-Christensen, E., & Wilhjelm, J. (1972). Interplanetary
 414 magnetic-field direction and high-latitude ionospheric currents. *Journal of*
 415 *Geophysical Research*, 77(10), 1976–1977. doi: <https://doi.org/10.1029/JA077i010p01976>
- 416
- 417 Khan, H., & Cowley, S. (1999). Observations of the response time of high-latitude
 418 ionospheric convection to variations in the interplanetary magnetic field using
 419 EISCAT and IMP-8 data. *Annales Geophysicae*, 17(10), 1306–1335. doi:
 420 <https://doi.org/10.1007/s00585-999-1306-8>
- 421 King, J., & Papitashvili, N. (2005). Solar wind spatial scales in and comparisons
 422 of hourly Wind and ACE plasma and magnetic field data. *Journal of Geo-*
 423 *physical Research: Space Physics*, 110(A2). doi: <https://doi.org/10.1029/2004JA010649>
- 424
- 425 Lockwood, M., & McWilliams, K. A. (2021). On optimum solar wind–
 426 magnetosphere coupling functions for transpolar voltage and planetary
 427 geomagnetic activity. *Journal of Geophysical Research: Space Physics*,
 428 e2021JA029946. doi: <https://doi.org/10.1029/2021JA029946>
- 429 Mansurov, S. (1969). New evidence of a relationship between magnetic fields in
 430 space and on earth. *Geomag. Aeron.*, 9, 622–623.

- 431 Milan, S., Baddeley, L., Lester, M., & Sato, N. (2001). A seasonal variation in the
432 convection response to IMF orientation. *Geophysical Research Letters*, *28*(3),
433 471–474. doi: <https://doi.org/10.1029/2000GL012245>
- 434 Milan, S., Carter, J., Korth, H., & Anderson, B. (2015). Principal component anal-
435 ysis of Birkeland currents determined by the Active Magnetosphere and Plane-
436 tary Electrodynamics Response Experiment. *Journal of Geophysical Research:*
437 *Space Physics*, *120*(12), 10–415. doi: <https://doi.org/10.1002/2015JA021680>
- 438 Milan, S., Carter, J., Sangha, H., Laundal, K., Østgaard, N., Tenfjord, P., ... oth-
439 ers (2018). Timescales of dayside and nightside field-aligned current response
440 to changes in solar wind-magnetosphere coupling. *Journal of Geophysical*
441 *Research: Space Physics*, *123*(9), 7307–7319. doi: <https://doi.org/10.1029/2018JA025645>
- 442
- 443 Milan, S., Clausen, L., Coxon, J., Carter, J., Walach, M.-T., Laundal, K., ... others
444 (2017). Overview of solar wind–magnetosphere–ionosphere–atmosphere cou-
445 pling and the generation of magnetospheric currents. *Space Science Reviews*,
446 *206*(1-4), 547–573. doi: <https://doi.org/10.1007/s11214-017-0333-0>
- 447 Milan, S., Gosling, J., & Hubert, B. (2012). Relationship between interplanetary pa-
448 rameters and the magnetopause reconnection rate quantified from observations
449 of the expanding polar cap. *Journal of Geophysical Research: Space Physics*,
450 *117*(A3).
- 451 Newell, P., Sotirelis, T., Liou, K., Meng, C.-I., & Rich, F. (2007). A nearly universal
452 solar wind-magnetosphere coupling function inferred from 10 magnetospheric
453 state variables. *Journal of Geophysical Research: Space Physics*, *112*(A1).
- 454 Svalgaard, L. (1973). Polar cap magnetic variations and their relationship with
455 the interplanetary magnetic sector structure. *Journal of Geophysical Research*,
456 *78*(13), 2064–2078. doi: <https://doi.org/10.1029/JA078i013p02064>
- 457 Waters, C., Anderson, B., Green, D., Korth, H., Barnes, R., & Vanhamäki, H.
458 (2020). Science data products for AMPERE. In *Ionospheric Multi-Spacecraft*
459 *Analysis Tools* (pp. 141–165). Springer, Cham. doi: https://doi.org/10.1007/978-3-030-26732-2_7
- 460
- 461 Waters, C., Anderson, B., & Liou, K. (2001). Estimation of global field aligned
462 currents using the Iridium® system magnetometer data. *Geophysical Research*
463 *Letters*, *28*(11), 2165–2168. doi: <https://doi.org/10.1029/2000GL012725>